nature photonics

SUPPLEMENTARY INFORMATION

DOI: 10.1038/NPHOTON.2017.35

In the format provided by the authors and unedited.

Single-photon imager based on a superconducting nanowire delay line

Authors: Qing-Yuan Zhao[1], Di Zhu[1], Niccolò Calandri[1,2], Andrew E. Dane[1], Adam N. McCaughan[1], Francesco Bellei[1], Hao-Zhu Wang[1], Daniel F. Santavicca[3], Karl K. Berggren[1*]

Affiliations:

[1]Massachusetts Institute of Technology, Department of Electrical Engineering and Computer Science, Cambridge, MA, 02139

[2]Politecnico di Milano, Department of Electronics, Information and Bioengineering, Milano, ITA, 22020

[3]University of North Florida, Department of Physics, Jacksonville, FL 32224

*Correspondence to: berggren@mit.edu

TABLE OF CONTENTS

1. Supplementary figures for the methods section

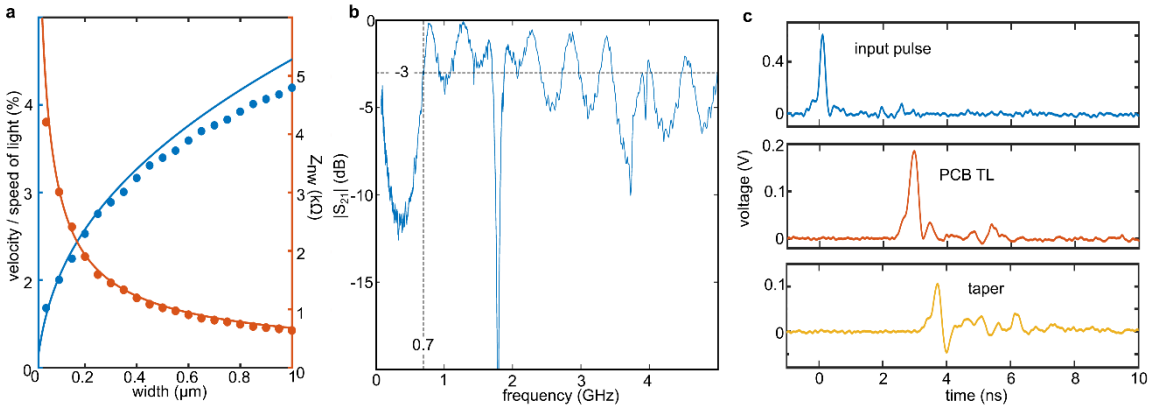

Supplementary Figure 1 | Microwave design of the SNSPI. a, Calculated velocity and impedance of superconducting coplanar waveguides with different widths. The sheet kinetic inductance of the wire is set to 50 pH/square. The dots are from numerical simulation while the lines are from analytical calculation. See Methods section for details about the geometry of the wire. **b**, Magnitude of the transmission coefficient $S_{21} = 20 \times \log(V_{out}/V_{in})$ of a 17.3-mm-long straight taper without connecting to a photon-sensitive nanowire, where V_{in} is the input signal to the taper from a network analyser and V_{out} is the measured output signal through the taper. The high-pass bandwidth starts at 0.7 GHz. The sharp dips close to 2 GHz and 4 GHz are likely due to resonances caused by the wire bonding connections between the chip and the print circuit board (PCB). **c**, Time domain measurement of the taper. We measured the transmitted pulse propagating through the taper and compared it to the transmitted pulse propagating through a 50 Ω PCB transmission line (TL). The comparison evaluates the amplitude loss and the pulse shape distortion of the transmitted pulse propagating through the superconducting taper.

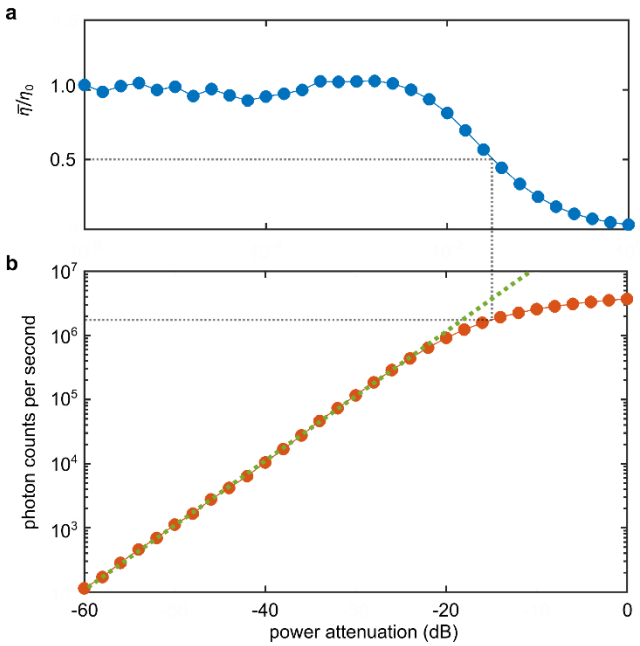

Supplementary Figure 2 | Maximum counting rate of the SNSPI. a. Normalized detection efficiency ($\bar{\eta}/\eta_0$) at different attenuations of the incident light. $\bar{\eta}$ is the average detection efficiency at different attenuations. η_0 is the detection efficiency when the device is fully reset to its initial bias current. We used a 1.5 μm continuous-wave laser and the readout circuit reported in ref. 1 to avoid the capacitive charging from RF amplifiers. **b**. The photon counts per second versus the attenuation of the incident light. The linear part, shown as the green line, gives η_0, where the inter arrival time of individual photons is longer than the current recovery time.

2. Imaging set-up and readout electronics

Here, we give the details of the electrical readouts and the optical setup for operating the SNSPI, which are shown in supplementary Fig. 3. We mounted the SNSPI and the imaged objects on a PCB board with two coaxial cables for connecting the device to room-temperature readout electronics. The PCB was mounted on a 2-inch lens tube which had a lens for collimating the laser beam. The SNSPI, imaged object, PCB and the tube were immersed in liquid helium at 4.2 K.

The room-temperature readout circuit was used for supplying the SNSPI with a DC bias current, amplifying the output pulses, and determining the pulse arrival times. We used two bias tees (Mini Circuits ZFBT-6GW+) to separate the DC and RF signals. As the SNSPI is a two-terminal device, we terminated one bias tee's DC port with a 50 Ω load and connected a voltage source (Stanford Research Systems, SRS 928) in series with a 10 kΩ resistor to the other bias tee's DC port. With this configuration, a DC current could go through the nanowire. Each bias tee's RF ports were connected to two cascaded RF amplifiers (RFbay LNA-2500 and Mini Circuit ZX60-3018G-S), offering a total gain of 47 dB and a bandwidth from 20 MHz to 2.5 GHz. The two output signals were acquired by a 6 GHz real-time oscilloscope (Lecroy Wavepro 760Zi). The oscilloscope was triggered on one of the output channels. The arrival times were recorded in the oscilloscope and then exported to a computer to process an image. To detect the arrival times of the electrical pulses, we set a constant discrimination threshold level on the pulse edges. Due to the existence of voltage noise that cause amplitude fluctuation of the pulse, the measured arrival times contained an excessive timing variation, which was defined as the system's electrical jitter j_e. We calculated $j_e = \delta_n/\rho$ from the measured waveforms of the pulses, where δ_n was the standard deviation of a Gaussian function fitting from the distribution of the measured noise in a 20 ns timing duration (a total of 801 points) and ρ was the slew rate at the discrimination threshold level. In our set-up, for each channel, j_e was 4.3 ± 0.6 ps, corresponding to a FWHM value of 10.1 ps ± 1.4 ps.

The light was prepared at room temperature and then illuminated on the device through a single-mode fibre (SMF-28) connecting to the lens tube. We used three light sources at different wavelengths, 405 nm, 780nm and 1.5 μm. The light was attenuated to ensure the device was operated at the single-photon level. The 1.5 μm source was a mode-locked laser (Calmar Laser

FPL-02CFF), offering sub-ps wide optical pulses at a repetition rate of 20 MHz. We used this source for characterising the temporal resolution of the SNSPI. In this measurement, the output of the laser was split into two: one illuminated the imager and the other one triggered a fast photodiode (Thorlabs DET08CFC) as a timing reference. The 780 nm light was a continuous-wave laser source (Thorlabs S1FC780), and the 405 nm light was a fibre-coupled continuous-wave light-emitting diode (Thorlabs M405F1). When the continuous-wave sources were used, the splitter and photodiode were removed.

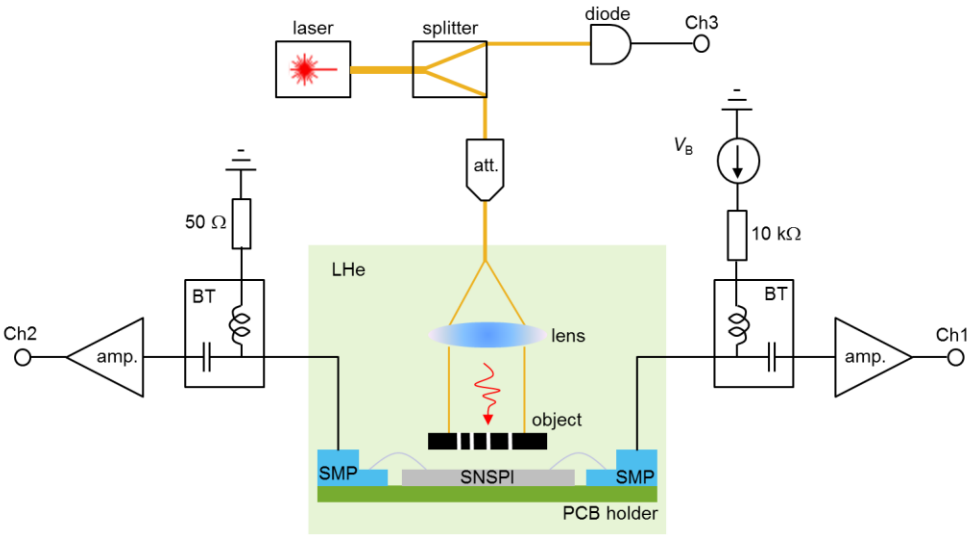

Supplementary Figure 3 | Detailed experimental set-up. A detailed description is in the Methods section 'set-up'. The abbreviations are: att. (optical attenuation), V_B (bias voltage source), BT (bias tee), amp (RF amplifier), SMP (SMP connector), Ch1~Ch3 (the input channels of an oscilloscope), LHe (liquid helium).

3. Wave propagation in a superconducting nanowire

In the SNSPI, as the thin superconducting nanowire has high kinetic-inductance, which dominates the overall inductance, the wave propagation in the SNSPI is qualitatively different from the wave propagation in conventional microwave waveguides, and shows similar

characteristics to a plasma wave. According to previous literature, a superconductor in the superconducting state can be treated as a plasmonic material with negative permittivity[2,3]. In the two-fluid model, the currents in a superconducting nanowire can be separated into two: the superconducting current carried by the superconducting electrons of a density n_s, and the normal current carried by normal electrons of a density n_n. Applying the Drude model, the relative dielectric constant $\varepsilon(\omega)$ of a superconductor below the gap frequency (usually a few THz) can be written as:

$$\varepsilon(\omega) = 1 - \left(\frac{\omega_s}{\omega}\right)^2 - \left(\frac{\omega_n^2 \tau_n^2}{\omega^2 \tau_n^2 + 1}\right) - j\left(\frac{\omega_n^2 \tau_n}{\omega^3 \tau_n^2 + \omega}\right)$$

where $\omega_s = \sqrt{\frac{n_s e^2}{m\varepsilon_0}}$ is the plasma frequency of superconducting electrons, $\omega_n = \sqrt{\frac{n_n e^2}{m\varepsilon_0}}$ is the plasma frequency of normal electrons (e is the elementary charge, m is the inertial mass of an electron and ε_0 is the permittivity in vacuum), and τ_n is relaxation time or the mean free time between collisions of normal electrons. At microwave frequencies, which are much lower than ω_n and ω_s, the normal electrons follow Ohm's law while superconducting electrons moves without resistance and have a kinetic energy of $\frac{1}{2} n_s m v_s^2$ (v_s is the velocity of the Cooper pairs). This kinetic energy is stored in an effective inductance. The kinetic inductivity is $\mathcal{L}_k = \frac{m}{n_s e^2} = \mu_0 \lambda_L^2$ (λ_L is the London penetration depth and μ_0 is the permeability). The plasma frequency ω_s then can be expressed as $\omega_s = \frac{c}{\lambda_L} = \sqrt{\frac{1}{\mathcal{L}_k \varepsilon_0}}$. In our experiments, the superconducting nanowire patterned from a ~7 nm thick niobium nitride film has a kinetic inductivity $\mathcal{L}_k = 3.4 \times 10^{-19}\ \mathrm{H \cdot m}$, giving $\omega_s =$ ~570 THz. ω_s is beyond the gap frequency of the Cooper pairs, indicating that within a wide bandwidth starting from very low frequency the superconducting

nanowire behaves as a plasmonic media of high kinetic inductance and negligible ohmic loss. At microwave frequencies, e.g., 10 GHz, the real part of the dielectric constant of the superconducting nanowire is ~-10^6. The major consequence of this characteristic is that the wavelengths of the guided waves were shortened. However, this behaviour is very different from plasmonic behaviour that is typically considered in, for example, surface plasmon polaritons.

4. Efficiency of the SNSPI and a microstrip SNSPI

To estimate the detection efficiency of the SNSPI demonstrated in the main article, we simulated the photon absorptance considering the coplanar structure. At 1550 nm, the light absorptance of the nanowire is 8% when light polarization is parallel to the nanowire, while it is 7% when light polarization is perpendicular to the nanowire.

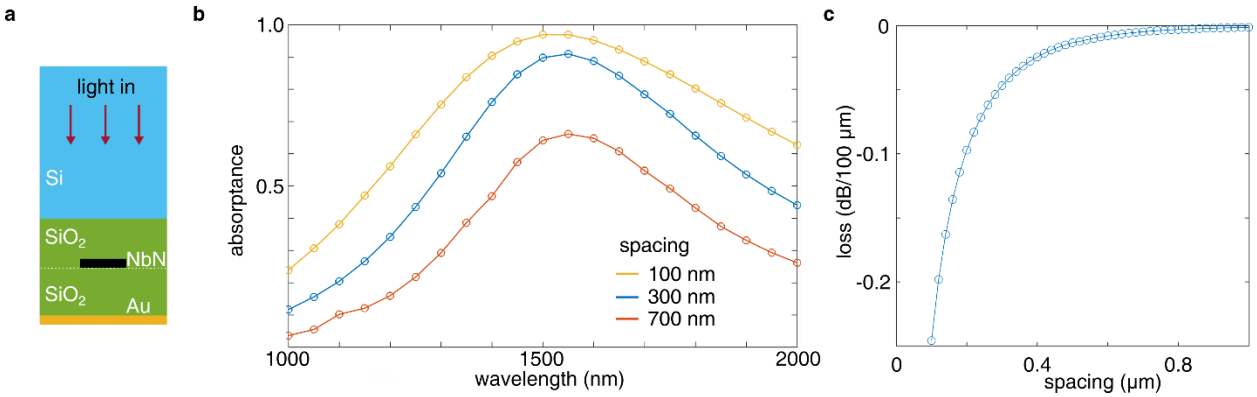

Supplementary Figure 4 | Simulation of a microstrip SNSPI. a. Material stack information in simulation. The light is stimulated inside the substrate to ignore the simulation of anti-reflected coating on the backside of the substrate. The nanowire is 6 nm thick. It is embedded in the centre of a 518 nm thick SiO2 layer. **b.** Simulated absorptance spectrum at different spacing between adjacent nanowires. The nanowire width is fixed at 100 nm. **c.** Simulated propagation loss due to crosstalk between adjacent nanowires. The two nanowires are both 100 nm wide and 100 μm long.

As we mentioned in the main article, a microstrip structure with an integrated optical cavity can enhance the detection efficiency of an SNSPI. In the microstrip structure shown in supplementary figure 4a, as the nanowire is fully embedded in a dielectric material (SiO_2), the

effective capacitance of the nanowire increases. For a 100 nm wide nanowire with a sheet inductance of 52 pH/sq, the calculated signal velocity reduces to 2% of the speed of light in free space.

In the microstrip structure, the filling factor of an SNSPI determines the trade-off between the absorptance and signal propagation loss. As shown in supplementary figure 4b and 4c, as the spacing between the adjacent nanowires increases from 100 nm to 700 nm, the absorptance peak reduces from 97% to 67% while the propagation loss reduces from -0.25 dB/100 μm to -0.0045 dB/100 μm.

5. Extended discussions of measured dark counts

The SNSPI enables a way to locate dark counts along the nanowire. However, as the 1D spatial resolution in our present SNSPI is 30 μm, which is larger than the period of bends (11 μm) of the meandered nanowire, the measured dark count peaks cannot accurately show whether the dark counts were generated at bends or constrictions along the nanowire.

The distribution of the dark counts over space is useful for estimating the homogeneity of an SNSPI[4]. We mapped the dark counts of the meandered nanowire and plotted the images in linear scale and logarithmic scales in supplementary figure 5(a) and (b), respectively. In the linear-scale image, dark counts are only localized to a few bright spots, supporting the idea that dark counts are from constrictions in a nanowire. In the logarithmic-scale image, there is a background where dark counts are two orders of magnitude lower than the bright spots, probably representing the intrinsic dark counts from uniform nanowires.

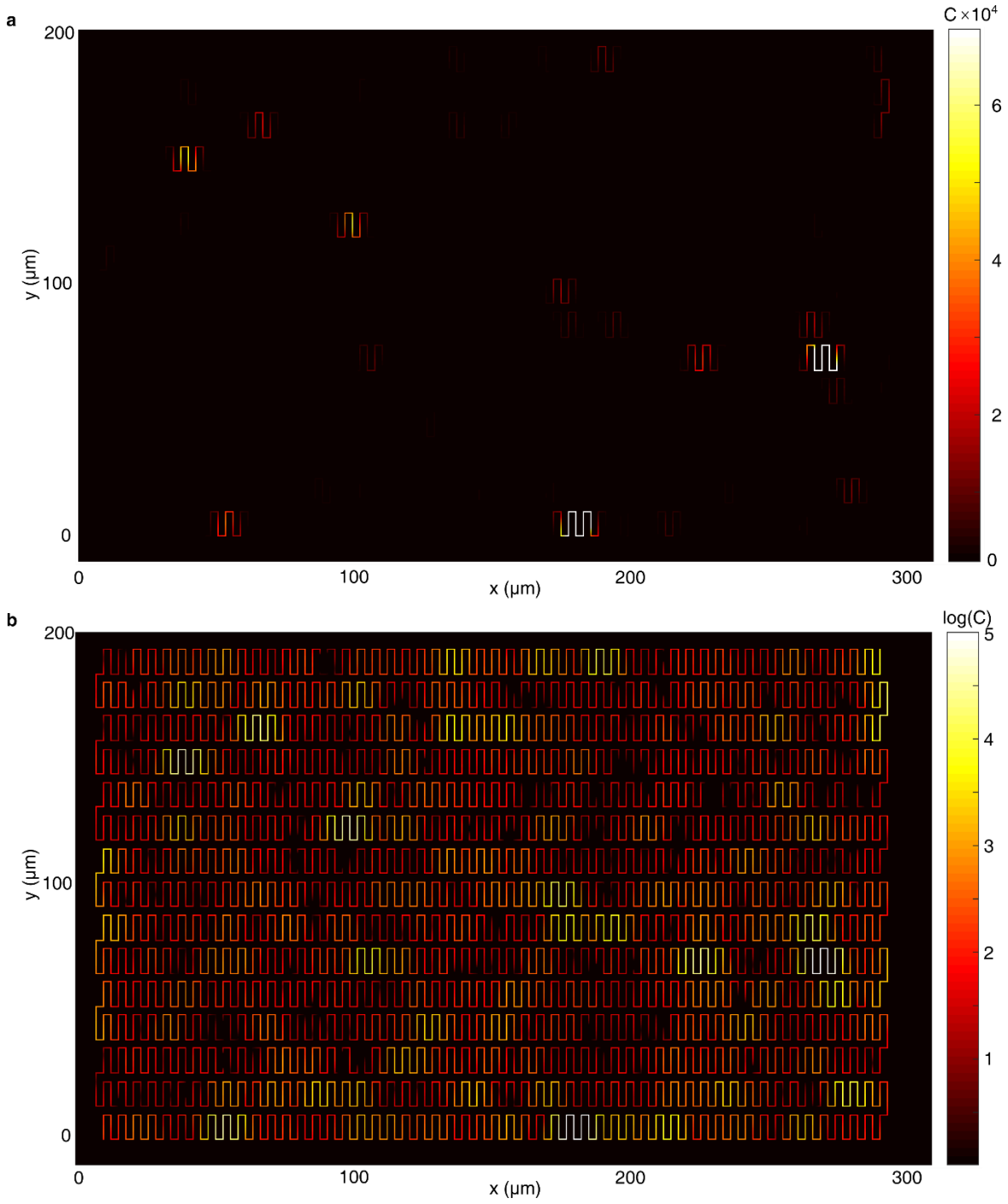

Supplementary Figure 5 | Dark counts mapped over the imaging area. The counts are plotted in linear scale **a** and logarithmic scale **b**.

6. References

1. Zhao, Q. *et al.* Counting rate enhancements in superconducting nanowire single-photon detectors with improved readout circuits. *Opt. Lett.* **39,** 1869 (2014).

2. Majedi, A. H. Theoretical investigations on THz and optical superconductive surface plasmon interface. *IEEE Trans. Appl. Supercond.* **19,** 907–910 (2009).

3. Tsiatmas, A., Fedotov, V. A., García de Abajo, F. J. & Zheludev, N. I. Low-loss terahertz superconducting plasmonics. *New J. Phys.* **14,** 115006 (2012).

4. Gaudio, R., op ’t Hoog, K. P. M., Zhou, Z., Sahin, D. & Fiore, A. Inhomogeneous critical current in nanowire superconducting single-photon detectors. *Appl. Phys. Lett.* **105,** 222602 (2014).